Geochemistry Geophysics Geosystems G3
AN ELECTRONIC JOURNAL OF THE EARTH SCIENCES
Published by AGU and the Geochemical Society

Article
Volume 4, Number 12
30 December 2003
9107, doi:10.1029/2003GC000540
ISSN: 1525-2027

Correction published 26 February 2004

Noble gas signatures of abyssal gabbros and peridotites at an Indian Ocean core complex

Hidenori Kumagai
Deep-Sea Research Department, Japan Marine Science and Technology Center (JAMSTEC), 2-15 Natsushim-cho, Yokosuka, 237-0061 Kanagawa, Japan (kumagai@jamstec.go.jp)

Henry J. B. Dick
Woods Hole Oceanographic Institution, Woods Hole, Massachusetts 02543, USA (hdick@whoi.edu)

Ichiro Kaneoka
Earthquake Research Institute, The University of Tokyo, Tokyo 113-0032, Japan (kaneoka@eri.u-tokyo.ac.jp)

[1] We report some of the first noble gas data for in situ lower oceanic crust and shallow mantle. From a suite of gabbros and peridotites recovered from the Atlantis Bank oceanic core complex on the Southwest Indian Ridge, we measured He, Ne, Ar, Kr and Xe concentrations as well as $^{3}He/^{4}He$ and $^{40}Ar/^{36}Ar$ ratios, there by documenting the noble gas content and signature of oceanic lithosphere. Except for a single ultramylonite, the gabbros have higher $^{3}He/^{4}He$ ratios than atmospheric. Three gabbros have MORB-like bulk $^{3}He/^{4}He$ ratios higher than $6R_A$ despite variable helium concentrations, as much as two to three orders of magnitude lower than in MORB glasses. One of these is mylonitized, demonstrating that magmatic helium can be retained despite intense high-temperature crystal-plastic deformation in the lower crust. Of the gabbros measured, green amphibole-bearing samples show relatively high helium abundances. Peridotite noble gas concentrations measured in clinopyroxene separates are dominantly lower than gabbros. Specifically, He abundances are similar to or greater than gabbros with MORB-like $^{3}He/^{4}He$ isotopic ratios. All the gabbros and peridotite clinopyroxenes show severely contaminated $^{40}Ar/^{36}Ar$ values up to 1300. Magmatic ^{40}Ar is enriched in the oxide-olivine gabbro with the highest $^{40}Ar/^{36}Ar$ in the entire sample suit. These results suggest as an actual data that the recycling of the lower oceanic crust and shallow mantle should be considered in modeling mantle evolution at least for helium. Measured helium abundances, though lower than in basalt glasses, are greater than those in crystalline MORB. Even if entire upper crust retains primary magmatic signature, oceanic lower crust and lithospheric mantle may impact larger by recycling due to their large volumes.

Components: 8337 words, 5 figures, 7 tables.

Keywords: $^{3}He/^{4}He$; Atlantis Bank; gabbro; clinopyroxene; high temperature alteration.

Index Terms: 1025 Geochemistry: Composition of the mantle; 1040 Geochemistry: Isotopic composition/chemistry; 1020 Geochemistry: Composition of the crust.

Received 4 March 2003; **Revised** 31 July 2003; **Accepted** 20 October 2003; **Published** 30 December 2003.

Kumagai, H., H. J. B. Dick, and I. Kaneoka, Noble gas signatures of abyssal gabbros and peridotites at an Indian Ocean core complex, *Geochem. Geophys. Geosyst.*, *4*(12), 9107, doi:10.1029/2003GC000540, 2003.

Theme: Accretionary Processes Along the Ultra-Slow Spreading Southwest Indian Ridge

Copyright 2003 by the American Geophysical Union

1. Introduction

[2] Noble gases have provided vital information on mantle evolution, both as a constraint on early mantle evolution and the formation of the continents, and as evidence for deep mantle plumes [*Porcelli et al.*, 2002]. Noble gases in the upper mantle are thought to be degassed, as mid-ocean ridge basalts (MORB) have higher $^{40}Ar/^{36}Ar$ ratios compared to those of ocean island basalt (OIB), showing that the latter have retained a more primitive noble gas signature. MORB $^{3}He/^{4}He$ values of $8R_A$ lie between those of OIBs and continental materials [cf. *Graham*, 2002] (R_A = atmospheric $^{3}He/^{4}He$ ratio of 1.4×10^{-6} [*Ozima and Podosek*, 1983]). The relatively uniform MORB helium isotopic ratio is believed to reflect the well-mixed nature of their source region, which appears to have undergone a prior melting event [*Graham*, 2002].

[3] There are very limited numbers of noble gas studies for in situ deep crust or mantle rocks [e.g., *Ozima and Podosek*, 1983], and no published data for abyssal gabbros and peridotites. This is mainly due to sampling difficulties and a dearth of fresh, unaltered material, especially abyssal peridotite. Even in the continental environment, limited studies have been made on in situ samples [e.g., *Drescher et al.*, 1998]. Instead, mantle-xenolith studies have been used to infer the noble gas signature of lithospheric mantle. A recent review by *Dunai and Porcelli* [2002] shows that the mean helium isotope ratio of subcontinental lithosphere determined from xenoliths is $6R_A$ - significantly different than that inferred for the oceanic lithosphere. However, they point out that this ratio may have been modified during transport from the mantle by contamination from the host magma as the host lavas could be derived from a different mantle source than the peridotite xenoliths.

[4] To better constrain the noble gas budget of the mantle, we have made some of the first noble gas measurements on gabbros and peridotites sampled in situ in the oceans. Surprisingly, despite the altered state of these rocks, they retain a mantle signature, at least for helium, and contain much higher concentrations than anticipated. Thus recycled lower ocean crust and shallow mantle can be a significant contributor to the lithospheric noble gas budget.

2. Sample Locality

[5] The Atlantis Bank core complex is the most extensively surveyed oceanic plutonic complex to date [*Dick et al.*, 1999a; *Hosford et al.*, 2003; *Matsumoto et al.*, 2002]. The complex consists of a roughly 800 km^2 gabbro massif exposed along a major north-south lineated bathymetric high flanking the Atlantis II Transform Fault on the Southwest Indian Ridge (SWIR, Figure 1). The gabbro massif is in contact at variable depths with mantle peridotite on its western flank along the transform wall.

[6] ODP Hole 735B is located at the top of the bank in the center of the gabbro complex. It penetrated 1500 m of intercalated coarse-grained olivine gabbro and subordinate ferrogabbro. Most of the section is undeformed or very weakly deformed with only a few percent alteration. Near the top of the Hole, however, the section is often mylonitized, and extensively altered at granulite to middle amphibolite facies conditions. Few primitive gabbros were drilled, and the average composition of the hole is too differentiated to represent in situ crystallization of primary MORB [*Dick et al.*, 2000]. U-Pb zircon ages of ~12 Ma were reported for Hole 735B by *John et al.* [2002].

[7] Our samples were collected with the submersible Shinkai 6500 and the ROV Kaiko on three separate cruises to Atlantis Bank during a joint investigation by the Japan Marine Science and Technology Center (JAMSTEC) and the Woods Hole Oceanographic Institution from 1998 to 2001. Locations are summarized in Table 1 and Figure 1. Five representative gabbros were selected at ~300 m depth intervals from a 4.8 km traverse that sampled 18 olivine and 11 intercalated oxide gabbros from a massive section of lower crust exposed on the transform wall at 32°38′S between 4001 and 2528 meters water depth. Two peridotites were also selected 50 m apart from the base of a 4.2 km traverse that sampled mixed plagioclase-bearing and plagioclase-free lherzolite and harz-

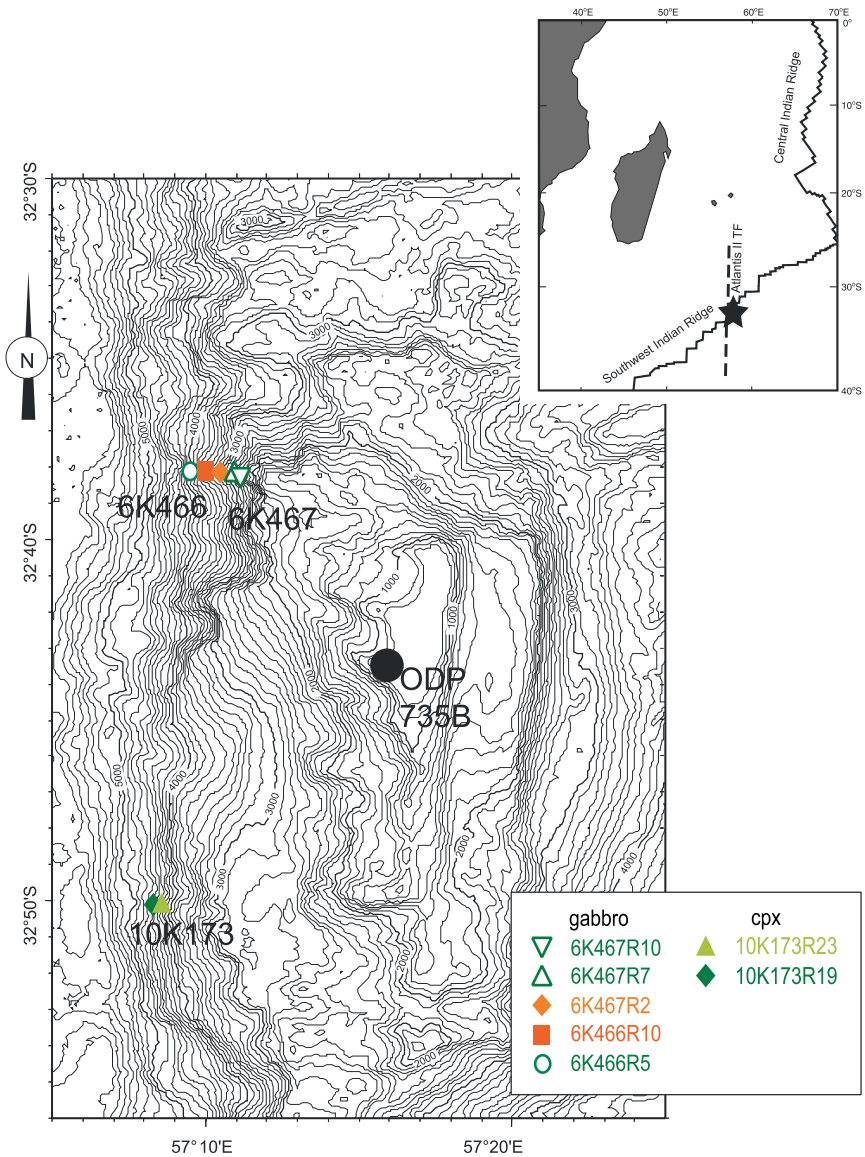

Figure 1. Sampling localities at Atlantis Bank, Indian Ocean. Symbols represent as follows. Open symbols, olivine gabbros; brown diamond, oxide olivine gabbro; square, oxide gabbro; filled triangle, lherzolite; green diamond, websterite. The position of ODP Hole 735B is also shown. An approximate position of Atlantis Bank is shown as a star in inset.

burgite from a massive mantle section exposed on the transform wall 3–4 km west of the main gabbro massif at 32°50′S between 5000 to 3000 m water depth.

3. Sample Description

3.1. Gabbros

[8] Two oxide gabbros (6K466R10 and 6K467R2) and three olivine gabbros (6K466R5 and 6K467R7, R10) were selected for analysis (Table 2). These rock names follow those of ODP Leg 176 [*Dick et al.*, 1999b].

[9] The oxide gabbros include an amphibolitized oxide gabbro ultramylonite (6K466R10) and an oxide-olivine gabbro mylonite (6K467R2). They consist largely of plagioclase and clinopyroxene with 3–15% ilmenite and titanomagnetite, though sample 6K467R2 contains a small amount of olivine now pseudomorphed by clay, and 2% brown

Table 1. Localities of Studied Samples

Sample	Sampled Position		Location	Water Depth
	Long.	Lat.		
		Gabbros		
6K467R10	57°11.120′E	32°38.132′S	Float	2528 m
6K467R7	57°11.018′E	32°38.162′S	On outcrop	2676 m
6K467R2	57°10.468′E	32°38.167′S	Float	3069 m
6K466R10	57°10.020′E	32°38.130′S	On outcrop	3375 m
6K466R5	57°09.560′E	32°38.130′S	Talus	4001 m
		Host Peridotites of Clinopyroxenes		
10K173R23	57°08.427′E	32°50.091′S	Outcrop	4509 m
10K173R19	57°08.394′E	32°50.094′S	Outcrop	4558 m

amphibole. Like many Atlantis Bank ferrogabbros, both exhibit strong crystal-plastic deformation. Plagioclase is 90–95% and clinopyroxene is 50–65% dynamically recrystallized. Alteration is mostly in the amphibolite facies, and is light in the oxide-olivine gabbro, but very heavy in the oxide gabbro. In the latter, clinopyroxene is entirely replaced by green amphibole and plagioclase is often turbid.

[10] The olivine gabbros contain ~60% plagioclase, 22–30% clinopyroxene, 10–18% olivine, <1% brown amphibole and <1% iron oxides. Olivine gabbro 6K466R5 shows no crystal-plastic deformation, 6K467R7 weak deformation and 6K467R10 moderate deformation with a good foliation. All three are quite fresh with olivine unaltered to 2% replaced by low temperature clays and chlorite, and plagioclase and pyroxene only 1–5% replaced by green amphibole and/or chlorite. Owing to the overall freshness of the coarser gabbros and the fine grain size of the mylonites, we analyzed only whole rock gabbros for this study.

3.2. Peridotites

[11] The peridotites include a granular websterite (10K173R19) and a protogranular lherzolite (10K173R23, Table 2). These textures are characteristic of the earliest high-temperature fabrics in abyssal peridotites, often associated with mantle melting beneath an ocean ridge. Textural elements, associated with lower temperature crystal-plastic deformation or cataclasis are minor. Plagioclase, indicative of crystallized trapped melt [*Dick*, 1989], was not observed in either peridotite. The websterite likely represents a mantle vein produced by melt impregnation at pressures above the plagioclase stability field, while the lherzolite is probably a simple residue of low degree mantle melting.

[12] The extent of alteration of the peridotites is substantial. Most olivine is replaced by serpentine, principally lizardite, though a significant proportion of primary enstatite and clinopyroxene has survived. In the lherzolite, 85% of the olivine is weathered to brown-colored clays and other secondary minerals. Trace sulfides are also observed, while pyroxene has few serpentine veins but abundant inclusions too small to identify. In the websterite abundant fibrous serpentine veins crosscut pyroxene, and carbonate and zeolite veins are also present. Therefore to avoid alteration effects, whole rock analyses were not made, and fresh clinopyroxene was separated from both samples and used in this study.

4. Analytical Procedures

[13] Gabbro fragments of ~1 g were cut and ultrasonically cleaned for 5 min with 1N- HNO_3 and rinsed with pure water, acetone and ethanol. To make the mineral separates the peridotites were crushed to less than one millimeter in size, sieved, and relatively clear and less-fractured clinopyroxenes were hand picked. These grains were then gently etched at 70°C for 30 min with 2N-HNO_3. After etching, discolored and fragmented clinopyroxene grains were removed by hand picking using a binocular microscope, reducing the volume of the lherzolite separate by 65% and the websterite separate by 25%. The remaining clear clinopyrox-

Table 2. Petrography of Analyzed Gabbros and Peridotites[a]

Sample Number	Lithology	Gr. Size, mm	Primary Igneous Mineralogy								Crystal-Plastic Recrystallization, %					Alteration, %			
			Plag	Cpx	Opx	Ol	Br Am	Tmt	Ct	Sulf	Plag	Cpx	Opx	Ol	Grade	Plag	Cpx	Opx	Ol
Gabbros																			
6K467R10[b]	Olivine Gabbro protomylonite	7.5	60	30	-	10	<1	Tr			90	80	-	95	3.5	1 Chl, Cl	-	-	1 Chl, Cl
6K467R7[c]	Olivine Gabbro	10	59	21	0.5	18	0.5	<1			5	-	-	-	0.5	2 grAm	2 grAm	-	2
6K467R2[d]	Oxide Olivine Gabbro mylonite	2 to 5	58	22	-	3	2	15			90	50	-	100	3.5	Tr Chl	1 grAm, 10 Cl	-	100 Id
6K466R10[e]	Oxide Gabbro ultramylonite	-	68	29	-	-	-	3			95	65	-	-	4.5	5?	100 grAm	-	-
6K466R5[f]	Olivine Gabbro	10	59	28	-	12	1	<1			1	-	-	-	0	5 Chl	-	-	-
Peridotites																			
10K173R23[g]	Protogranular Lherzolite	7.5	-	10	28	62	-	-	1	Tr	-	-	-	-	0	-	10 Serp	25 Serp	85 Serp
10K173R19A[h]	Granular Websterite	5	-	69	20	10	-	-	1	-	-	20	-	-	1.5	-	10 Serp	60 Serp	80 Serp

[a] Mineral abbreviations: Plag, plagioclase; Cpx, clinopyroxene; Opx, orthopyroxene; Ol, olivine; Br Am, brown amphibole; Tmt, titanomagnetite; Ct, chromite; Sulf, sulfide. Deformation grade runs from 0 to 5, with 0 undeformed to 5 ultramylonite. Alteration minerals: grAm, green amphibole; Chl, chlorite; Cl, clay; Serp, serpentine.
[b] Sample contains a few thin chlorite and smectite veins and about 2% clay. Well foliated.
[c] Thin late magmatic vein of recrystallized gabbro impregnated with brown amphibole.
[d] A few zircons present.
[e] Contains dark green amphibole veins perpendicular to the well developed foliation. Coarse to medium pyroxene porphyroclasts abundant. Locally has 1–2% iron-oxide stained thin clay filled cracks. Trace of apatite. Plagioclase is clear, but locally very turbid filled with 5–20% small micro-inclusions. Could be fine clay or chlorite.
[f] Sample contains some thin brown clay stained cracks and veins.
[g] Some small irregular interstitial clinopyroxenes that look like they were melt-impregnated.
[h] Contains cross fiber serpentine veins up to 2 mm, a 1 mm carbonate vein with mineral fragments, and a 1 mm zeolite vein running along side the carbonate vein.

Table 3. Noble Gas Abundances, $^{3}He/^{4}He$ and $^{40}Ar/^{36}Ar$ of Gabbros and Peridotites[a]

Sample Weight, g	T, °C	^{4}He, ncc/g	^{20}Ne, ncc/g	^{36}Ar, ncc/g	^{40}Ar, μcc/g	^{84}Kr, pcc/g	^{132}Xe, pcc/g	$^{40}Ar^{*}$, μcc/g	$^{4}He/^{40}Ar^{*}$	$^{3}He/^{4}He$ (R_A)	±	$^{40}Ar/^{36}Ar$	±
						Gabbro							
6K467R10	900	13.29	0.0524	0.277	0.0887	20.7	2.18			4.98	0.66	320.3	7.6
Ol-Gb	1700	9.65	0.0357	0.1345	0.0574	10.94	1.966			9.10	0.93	426	11
1.3685	Total	22.9	0.0880	0.411	0.1461	31.7	4.15	0.024	0.94	6.71	0.57	355.0	6.6
6K467R7	900	99.5	0.287	0.269	0.1131	14.53	1.248			8.10	0.29	420.8	9.3
Ol-Gb	1700	35.0	0.0300	0.0960	0.0615	5.90	2.67			7.87	0.44	638.8	7.1
1.6349	Total	134.5	0.317	0.365	0.1746	20.4	3.92	0.067	2.01	8.05	0.25	478.7	9.9
6K467R2	900	40.7	9.71	3.62	1.456	112.3	1.763			3.80	0.19	402.4	9.3
Ox-Ol-Gb	1700	48.6	0.0396	0.555	0.716	72.5	3.77			8.52	0.47	1290	31
1.0426	Total	89.3	9.75	4.17	2.17	184.8	5.53	0.94	0.10	6.37	0.32	520	53
6K466R10	900	63.6	1.776	1.905	0.581	74.1	2.25			0.165	0.029	305.2	6.9
Ox-Gb	1700	4.15	0.0493	0.478	0.1644	27.1	2.34			1.07	0.24	344.1	7.9
0.9828	Total	67.8	1.825	2.38	0.746	101.2	4.60	0.042	1.63	0.220	0.031	313.0	5.7
6K466R5	900	15.11	0.241	0.317	0.1142	15.16	1.071			2.90	0.18	360.5	7.4
Ol-Gb	1700	4.02	0.1743	0.1374	0.0713	7.64	0.806			7.66	0.62	519	16
1.8357	Total	19.14	0.416	0.454	0.1856	22.8	1.877	0.051	0.37	3.90	0.23	408.6	8.2
						Clinopyroxenes of Peridotites							
10K173R23	700	51.7	0.0128	0.0845	0.0297	6.25	1.712			8.11	0.47	352.0	7.7
Lherzolite	1200	106.9	0.0242	0.0814	0.0303	6.34	0.903			8.38	0.41	372.1	7.3
0.4677	1750	0.13	0.0400	0.1942	0.0651	15.90	2.05			8.06	0.40	335.0	6.3
	Total	158.7	0.0771	0.360	0.1251	28.5	4.66	0.019	8.50	8.30	0.31	347.4	4.2
10K173R19	700	3.07	0.0124	0.0331	0.0116	2.05	1.225			4.73	0.87	350	21
Websterite	1200	27.6	0.0309	0.0527	0.0247	2.68	0.444			8.50	0.44	468.6	11.3
0.6830	1750	n.d.	0.0252	0.0514	0.0227	2.80	0.555			-		441.9	17.0
	Total	30.7	0.0684	0.1373	0.0590	7.53	2.22	0.018	1.66	8.13	0.41	430.0	9.2

Typical Blank	°C	ncc	ncc	ncc	μcc	pcc	pcc
Gabbro	900	0.09	0.0009	0.0005	0.0002	0.01	0.002
measurement	1700	0.14	0.0052	0.0031	0.0009	0.10	0.029
Clinopyroxene	700	0.10	0.0044	0.0009	0.0003	0.04	0.003
measurement	1200	0.10	0.0047	0.0008	0.0002	0.03	0.005
	1750	0.07	0.0034	0.0018	0.0005	0.06	0.011

[a] n.d.: significantly lower than blank level; dash indicates not analyzed. Experimental uncertainties in amounts are generally about 5% for Ar and 10% for the others (2σ), respectively, estimated from the air calibration reproducibility. Typical variations in blank levels are less than 25%, 30% and 33% for up to 1000°C, 1200°C and above 1700°C fractions, respectively. Primary lithologies of gabbros are represented as follows. Ol-Gb, Olivine gabbro; Ox-Ol-Gb, Oxide olivine gabbro; Ox-Gb, Oxide gabbro.

enes were then ultrasonically cleaned with distilled water, acetone and ethanol. Prior to gas extraction, all samples were baked at 150°C in vacuum.

[14] Noble gas analyses were performed with a VG-5400 noble gas mass spectrometer installed in Earthquake Research Institute of the University of Tokyo. Stepwise heating was used with two temperature steps for gabbros and three for clinopyroxene separates to extract the gases (Table 3). Details of analysis are described in *Hanyu et al.* [1999]. Major elements as well as Ba, Sr, Y, Sc, Zr, Be and V were obtained by lithium metaborate/tetraborate fusion ICP analysis, while REE and 29 additional trace elements analyses were obtained by ICP-MS at Activation Laboratories of Ancaster, Canada. Details are described in Appendix.

5. Helium

5.1. MORB-type $^{3}He/^{4}He$

[15] Concentration weighted 'total' He compositions of clinopyroxenes separated from abyssal peridotites fall within the commonly held MORB-type benchmark of 8 ± 1R_A. In particular, lherzolite 10K173R23 clinopyroxene shows uniform $^{3}He/^{4}He$ within analytical uncertainty (ca.

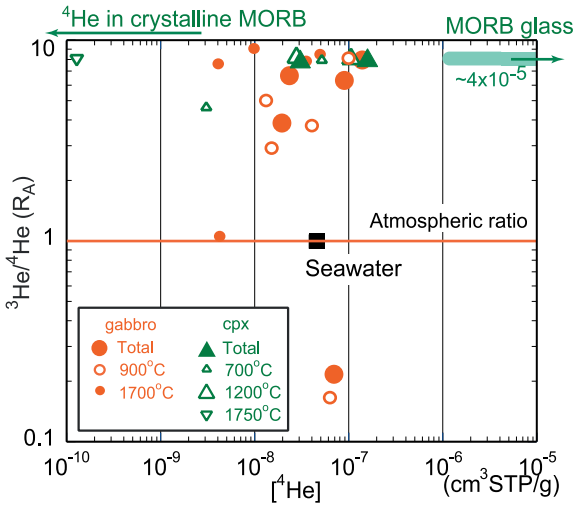

Figure 2. Result of helium measurements. Gabbro: The larger filled circles show bulk values of stepwise heating. Open circles and smaller filled circles show values of 900°C and 1700°C fractions, respectively. Clinopyroxene of Peridotite: The larger filled triangles show bulk values of stepwise heating. The open triangles show the values of each fraction; small, large and inverted triangles show values of 700°C, 1200°C and 1750°C fraction, respectively. Hatched area shows the typical ranges of MORB glasses. As ^{3}He in crystalline MORBs frequently are under the detection limit, an arrow just above the upper horizontal axis shows their range of ^{4}He amount. The filled square represents helium composition of seawater.

±0.4 R_A in range) for all three temperature steps. Olivine gabbro 6K467R7 also shows MORB-type ^{3}He/^{4}He for both 900°C and 1700°C fractions (8.1 and 7.9 R_A). Except for the extremely altered oxide gabbro ultramylonite (6K466R10), the remaining three gabbros had MORB-like ^{3}He/^{4}He ratios of almost 8 R_A or above in the 1700°C fraction, regardless of helium concentration (Figure 2). This includes the mylonitized oxide-olivine gabbro 6K467R2, which has ^{3}He/^{4}He, 8.52 R_A in the 1700°C fraction. These results show that oceanic gabbros and peridotites can preserve the primary magmatic helium signature of the MORB source, even within highly deformed rocks.

5.2. Radiogenic ^{3}He/^{4}He in Oxide Gabbro Ultramylonite 6K466R10

[16] Oxide gabbro ultramylonite 6K466R10 is unique in having a very low bulk ^{3}He/^{4}He of 0.22 R_A. The 1700°C gas fraction is atmospheric (^{3}He/^{4}He = 1 R_A), with a ^{4}He concentration of 4×10^{-9} cm^{3}STP/g. This apparent atmospheric helium ratio, however, does not likely represent seawater helium incorporated into metamorphic amphibole. The ^{4}He/^{20}Ne ratio of the 1700°C gas fraction reaches 100, while the ratio of seawater is only 0.4. Thus this 'atmospheric' ^{3}He/^{4}He ratio seems to be generated by a chance mixture of mantle He and ingrowth of radiogenic He. The 900°C fraction has a much more radiogenic (^{4}He-rich) isotopic composition of 0.165 R_A, supporting this interpretation. Normal in situ decay of U and Th gives pure ^{4}He, which, combined with associated very small ^{3}He contributions by following nuclear reactions, gives values of ~0.02 R_A [*Graham*, 2002] for helium isotopic ingrowth. The Th and U contents of this sample (0.17 and 0.23 ppm respectively) would produce the observed accumulation of ^{4}He (6.7×10^{-8} cm^3 STP/g) in 2 Ma. If all the ^{4}He produced by decay of the observed Th and U in the sample were preserved over the ~11 Ma age of the sample locality, the accumulation of ^{4}He would have reached 3.5×10^{-7} cm^3 STP/g. An equivalent accumulation of ^{40}Ar, as discussed later, has also been found, and can be similarly explained by decay of ^{40}K.

5.3. Helium Abundances

[17] Although the total helium abundances in all our samples are lower than those of MORB glasses by two to three orders of magnitude, these abundances are still significantly higher than those of crystalline MORBs (Figure 2). Bulk helium in the lherzolite clinopyroxene is also 5 times higher than in the websterite clinopyroxene. Although the degree of alteration is similar, clinopyroxene in the websterite is dominantly recrystallized and contains abundant fibrous serpentine veins. These textural differences may greatly impact the helium content of the respective clinopyroxene, though one must also consider the petrogenetic origin of host peridotite as well.

[18] In either case, however, clinopyroxene helium abundances are much higher than those anticipated from partitioning of helium with MORB magmas as represented by glassy MORBs with typical helium contents of 10^{-5} cm^3 STP/g [e.g., *Honda*

and Patterson, 1999]. Even in natural samples, the presence of inclusions does not guarantee that noble gas abundance is completely controlled by partitioning; helium is believed to be a highly incompatible element [e.g., *Graham*, 2002]. This view is supported by both laboratory high-pressure experiments and by comparisons between coexisting glass and phenocryst compositions in natural samples. For example, *Brooker et al.* [2003] reports extremely low partition coefficients between clinopyroxenes and coexisting glass for Ne with the value lower than 10^{-3}. Their data implies a helium mineral/melt partition coefficient close to 10^{-4}, under inclusion-free condition. However, glasses from the unique popping rocks dredged on the MAR contain great amounts of helium up to almost 10^{-4} cm^3 STP/g [*Moreira et al.*, 1998]. While trace element signatures are enriched relative to N-MORB, these He concentrations for undegassed MORB melts ('popping rock') would suggest that most MORB magmas lose 90% of their helium prior to glass solidification as an upper limit [*Sarda and Moreira*, 2002]. Even if this is the case, the partition coefficient between MORB melt and residual clinopyroxene will be 10^{-3}. The required value, however, would still be higher. If, on the other hand, their model provides a lower limit for He concentrations in primary MORB magmas, the He abundance in the peridotite clinopyroxenes can be explained by equilibrium with MORB magma prior to losing their primordial volatiles.

[19] Our gabbros contain the equivalent or smaller amounts of helium than the peridotite pyroxenes. The most abundant MORB-type helium was found in a lightly deformed and weakly altered olivine gabbro, 6K467R7. The oxide-olivine gabbro mylonite 6K467R2, however, retains significant amounts of MORB-like helium despite the degree of deformation. The Atlantis Bank oxide-olivine gabbros crystallized from highly differentiated iron-titanium-rich melts (~70% plus crystallization, *Natland and Dick* [2001]). Thus the high retained-helium abundance in this sample likely relates to a high initial content due to enrichment of the melt in volatiles during differentiation.

[20] Within the gabbros, the green amphibole-bearing samples (6K466R10, 6K467R2 and R7) show significantly higher helium contents regardless of isotopic composition. This suggests that amphiboles could be a principal host for noble gases, at least for helium. Green amphibole may form either deuterically or due to seawater alteration, and thus could host either magmatic or seawater volatiles. The remaining olivine gabbros are characterized by low helium concentration and low $^3He/^4He$ in the lower temperature fraction. One (6K467R10) is highly deformed while the other (6K466R5) is undeformed, and both are relatively fresh. They do have small amounts of brown magmatic amphibole, but neither has green amphibole, containing small amounts of chlorite instead. The low overall helium concentration, then, could relate to the absence of green amphibole, while magmatic helium retained in brown amphibole could account for greater than atmospheric $^3He/^4He$.

[21] Although our sample set is small, and a larger data set would be more definitive, the helium abundances of gabbros in the present study can be interpreted as a result of equilibration with MORB magma during their precipitation and solidification, modified to some extent by later alteration. Evidence for a correlation to degree of deformation is weak at best, though relative amphibole abundances suggest the possibility that this phase may be a host for helium in the gabbros.

6. Other Noble Gases

6.1. $^{40}Ar/^{36}Ar$

[22] $^{40}Ar/^{36}Ar$ ratios are low compared to typical MORB and range from 1290 down to 305 near the atmospheric value of 295.5, indicating only a little non-atmospheric ^{40}Ar (Figure 3). While many MORBs have $^{40}Ar/^{36}Ar$ ratios in the range of a few hundred to a few thousand [e.g., *Sarda et al.*, 2000; *Graham*, 2002], pristine MORB magmas are widely regarded as those with $^{40}Ar/^{36}Ar$ values exceeding 10,000. As all these samples have a high ^{36}Ar concentration, they appear to be severely contaminated by an atmospheric component.

[23] Non-atmospheric ^{40}Ar ($^{40}Ar^*$), calculated by subtraction of atmospheric ^{40}Ar (295.5 times of ^{36}Ar) from total ^{40}Ar is highly variable in the five

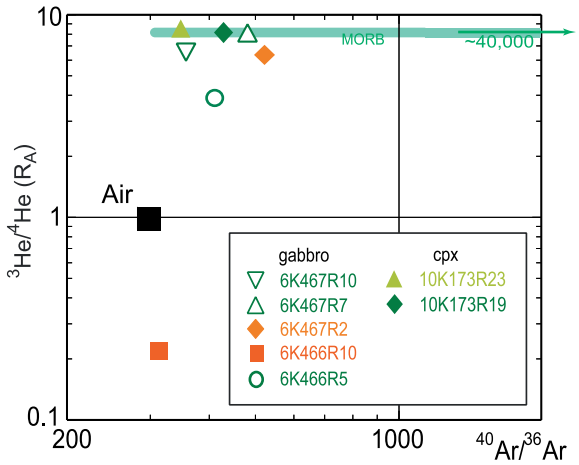

Figure 3. $^{40}Ar/^{36}Ar$ versus $^{4}He/^{3}He$ diagram. Symbols of samples are the same as Figure 1. The bulk values of stepwise heating are shown. The high end of MORB $^{40}Ar/^{36}Ar$ values is extended beyond the diagram, as its maximum is shown to be 40,000 [*Burnard et al.*, 1997]. The large filled square represents the value for seawater.

gabbros. Measured K_2O values in the gabbros range from 0.08 to 0.21 wt.% (Table 4). Except for olivine gabbro 6K467R10 with the lowest $^{40}Ar^*$, both the remaining olivine gabbros show significantly higher $^{40}Ar^*$ than that expected for in situ accumulation by decay of ^{40}K in 12 Ma. Oxide-gabbro ultramylonite 6K466R10 has an amount of $^{40}Ar^*$ roughly equivalent to that expected for in situ accumulation. Also lacking excess ^{4}He, this sample possibly lost its magmatic noble gases during alteration.

[24] Oxide-olivine gabbro 6K467R2 has a unique signature: while it contains the highest K_2O content (0.21 wt.%), its $^{40}Ar^*$ content reaches almost 1×10^{-6} cm^3 STP/g–11 times higher than the possible accumulation of $^{40}Ar^*$ over 12 Ma. This gabbro also shows the highest $^{40}Ar/^{36}Ar$, and has the second highest helium content measured. This amount of $^{40}Ar^*$ is equivalent to the excess argon found in zero age MORB glass, and the elevated $^{40}Ar/^{36}Ar$ in sample 6K467R2 likely comes from its parental magma.

[25] K_2O in abyssal peridotites is generally below detection limits for EPMA, however, assuming a K_2O content of 30 ppm up to $1.4 \times 10^{-9}$$cm^3$ STP/g of $^{40}Ar^*$ could accumulate in the pyroxene over 12 Ma. This is lower by an order of magnitude than observed $^{40}Ar^*$ in the pyroxene separates. Therefore the large observed differences in $^{4}He/^{40}Ar^*$ in the lherzolite and websterite clinopyroxene separates could be primary mantle or magmatic signatures reflecting the differences in their petrogeneses.

6.2. Elemental Abundances and Atmospheric Neon, Krypton and Xenon

[26] The noble gas elemental abundance patterns, with the exception of He and Ne, have similar shapes to those of glassy MORBs, and equivalent or higher heavier noble gas contents (Figure 4). Helium has concentrations lying between crystalline and glassy MORB, departing from both patterns. Neon shows a variable depletion relative to the 'smooth' MORB pattern, ranging from almost none for oxide-olivine gabbro mylonite 6K467R2 to one order of magnitude in olivine gabbro proto-

Table 4. Possible In Situ Accumulation of ^{4}He and ^{40}Ar in 12 Ma[a]

Sample	U, ppm	Th, ppm	In Situ ^{4}He (10^{-8} cm^3 STP/g)	Measured ^{4}He (10^{-8} cm^3 STP/g)	K_2O, wt%	In Situ ^{40}Ar (10^{-8} cm^3 STP/g)	Measured $^{40}Ar^*$ (10^{-8} cm^3 STP/g)
				Gabbros			
6K467R10	<0.01	<0.05	<3.15	2.3	0.12	4.76	2.4
6K467R7	<0.01	<0.05	<3.15	13.4	0.08	3.17	6.7
6K467R2	0.24	<0.05	<36.4	8.9	0.21	8.33	94
6K466R10	0.23	0.17	39.1	6.7	0.12	4.76	4.2
6K466R5	0.13	0.28	28.4	1.9	0.09	3.57	5.1
				Clinopyroxene Separates of Peridotites			
10K173R23	0.01	<0.01	<1.79	15.8	N.A.	-	1.9
10K173R19	N.A.	N.A.	-	3.1	N.A.	-	1.8

[a] N.A., not analyzed.

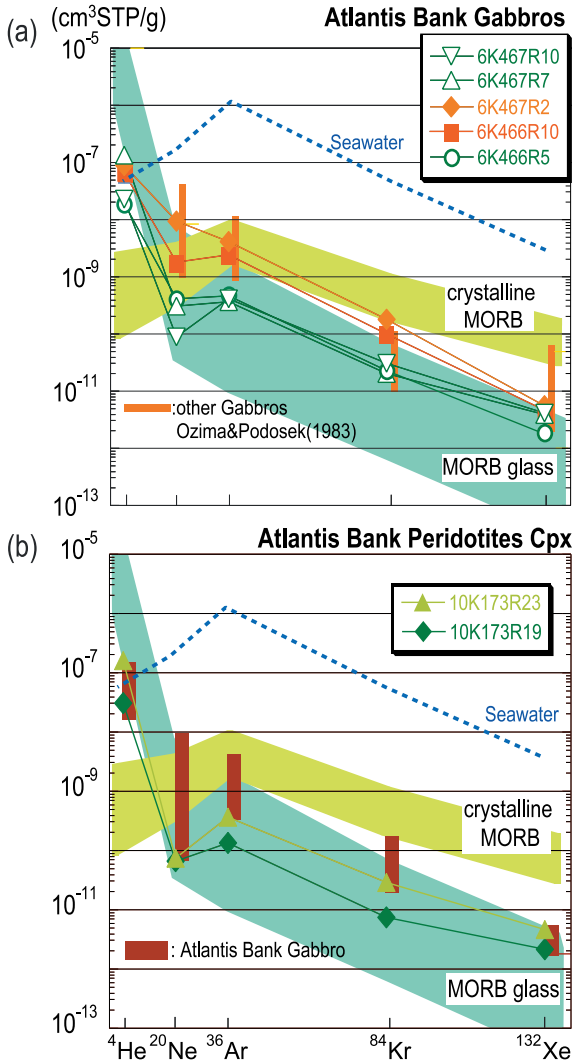

Figure 4. Noble gas abundance patterns (a) for gabbros and (b) for clinopyroxene separates of peridotites plotted as bulk values. In Figure 4a, open symbols represent olivine gabbros. Other symbols are the same as in Figure 1. The abundance pattern of deep seawater (Seawater) is also plotted as a broken line. Hatches show the typical range of glassy or crystalline MORBs. For comparison, the range of previously studied gabbros is shown by bars in Figure 4a [*Ozima and Podosek*, 1983]. Bars in Figure 4b also show the range of our gabbro samples.

mylonite 6K467R10. Xenon contents are as high as the most xenon-rich glassy MORBs, while the abundances of ^{36}Ar and ^{84}Kr are lower in the olivine gabbros than the highly evolved oxide gabbros.

[27] The Websterite and lherzolite have virtually identical noble gas patterns to the olivine gabbros, but differ significantly from the highly evolved oxide gabbros. The latter have higher absolute abundances for most of the noble gases, and significantly less depletion in ^{20}Ne relative to MORB glasses. The clinopyroxene separates have slightly lower neon and argon abundances than those of the lowest gabbro value (Figure 4b), while their ^{132}Xe contents are virtually identical. Lacking of comprehensive information on the partitioning of noble gases between pyroxene and olivine, it is difficult to interpret differences in the absolute elemental abundances between the gabbro whole rock analyses and the peridotite mineral separates.

[28] Although not shown in Table 3, the individual isotopic compositions measured for neon, krypton and xenon in our samples are all atmospheric as in MORB with low ^{40}Ar/^{36}Ar. Considering this, the departures in the noble gas patterns in Figure 4 from seawater must relate to contamination or hydrothermal alteration processes.

7. Discussion

7.1. Noble Gas Budgets in Lithospheric Mantle

[29] Our results show that the contribution of gabbroic lower crust to the lithospheric helium inventory is equal to or greater than that of pillow lavas and diabase, while the shallow mantle may potentially provide a reservoir with an even larger amount of helium (Table 5). This is because sea-floor basalts usually lose most of their magmatic helium except for a thin quenched glassy rind [*Dymond and Hogan*, 1973; *Kumagai and Kaneoka*, 1998]. Typically, the rinds are a few millimeters or less in thickness and likely comprise only 1% of a typical lava flow. Given that roughly half the earth's surface is normal oceanic crust (2.6×10^8 km^2), these rocks may contribute significantly to the lithospheric helium budget. Presuming a uniform 5 km thick gabbroic lower crust gives a volume exceeding1.3×10^9 km^3, and a mass of $\sim 4 \times 10^{24}$ g. Our measured gabbro He abundances, exceed 1×10^{-7} cm^3 STP/g. If this is taken as an average estimate, as much as 5×10^{17} cm^3 STP of MORB-type helium could be contained in the oceanic lower crust, equivalent to 2.5% of atmospheric helium.

Table 5. Estimated Noble Gas Budget/Inventory in Various Reservoirs

Reservoir	Mass, g	^{4}He, cm^{3}STP	$\times 10^{-9}$ cm^{3}STP/g	^{36}Ar, cm^{3}STP	$\times 10^{-8}$ cm^{3}STP/g	^{132}Xe, cm^{3}STP	$\times 10^{-11}$ cm^{3}STP/g
Oceanic crust (upper)	1×10^{24}	$\sim 4 \times 10^{17}$[a]	0.1–40000	$\sim 1 \times 10^{16}$	0.2–1.0	0.2–2.0 $\times 10^{14}$	2–20
Oceanic crust (lower)	4×10^{24}	0.8–5.2 $\times 10^{17}$	20–130	$<1.6 \times 10^{16}$	0.04–0.4	0.8–2.4 $\times 10^{13}$	0.2–0.6
Lithospheric mantle	5×10^{25}	1.5–8.0 $\times 10^{18}$	30–160	$< 2.0 \times 10^{16}$	0.01–0.04	1.0–2.5 $\times 10^{14}$	0.2–0.5
Upper mantle	1×10^{27}	$\sim 1 \times 10^{22}$	$\sim$10000[b]	$\sim 1 \times 10^{17}$	$\sim$0.01[b]		
Air	(5.119×10^{21})	2.08×10^{19}	(3.47)[c]	1.245×10^{20}	(2.08)[c]	9.27×10^{16}	(1.551)[c]

[a] Crystalline MORB with 1% of glassy portion were used for estimation.
[b] Estimated by *Porcelli and Ballentine* [2002].
[c] Atmospheric inventory were devided by the mass of the earth (5.976×10^{27}).

[30] The peridotites analyzed provide a first look at the possible contribution of the oceanic upper mantle to the lithospheric noble gas budget. Both were emplaced to the seafloor at the rift valley wall of the paleo-SWIR on the western flank of the core complex close to 12 Ma. Trace element abundances in lherzolite 10K173R23, specifically depleted LREE patterns (Y. Nishio, personal communication, 2003), indicate generation from low to moderate degrees of mantle melting similar to those reported by *Johnson and Dick* [1992]. Websterite 10K173R19 likely represents late-stage impregnation by ambient melt near the base of the lithosphere. Because they are the only available helium abundance of clinopyroxene in abyssal peridotite, we assume that they could represent possible upper and lower bounds for helium contents for the shallow oceanic mantle far from a hot spot. They span nearly the entire range of helium contents found in the gabbros, and both exhibit high ^{3}He/^{4}He ratios essentially identical to MORB. Given that MORB is thought to represent ~8–20% mantle melting [*Klein and Langmuir*, 1987], by inference the residual mantle is 5 to 13 times the volume of the entire crust. Thus the shallow oceanic mantle is potentially a major component of the lithospheric helium budget, and may contain a volume of helium equal to half that found in the earth's atmosphere. However, undegassed upper mantle should have as 10^3 times much helium as lithospheric and atmospheric inventories (Table 5).

[31] Unlike helium, with the exception of xenon, our measurements do not suggest a major reservoir for the other noble gases in the shallow earth, as their abundances are too low. For example, the undegassed MORB source has been estimated to contain 1×10^{-10} cm^3 STP/g of ^{36}Ar [*Porcelli and Ballentine*, 2002], which seems to be possible maxima results in 1×10^{-9} cm^3 STP/g of ^{36}Ar in glassy MORB. If this is the case, 1×10^{17} cm^3 STP of ^{36}Ar resides in the MORB source region at most. This value is three orders of magnitude lower than that of atmospheric ^{36}Ar.

[32] Our peridotites contain on the order of 10^{-12} cm^3 STP/g of ^{132}Xe with an atmospheric isotopic composition. Using this value, lithospheric oceanic mantle could contain up to 2.5×10^{14} cm^3 STP of ^{132}Xe, equivalent to 0.25% of the total atmospheric budget. If the oceanic lithosphere is recycled back into the mantle every ~200 Ma, 5×10^{15} cm^3 STP of ^{132}Xe, roughly 5% of total atmospheric inventory, could have been recycled back into the earth. This impact is similar to that by the upper crust including sediments.

7.2. ^{3}He/^{4}He of the Lower Temperature Fractions

[33] With the exception of one olivine gabbro with abundant helium, and the lherzolite clinopyroxene separate, our samples show lower ^{3}He/^{4}He in the 900°C and 700°C low-temperature fractions respectively. Generally, samples with smaller helium contents have lower ^{3}He/^{4}He in the low-temperature fraction. These values spread downward from MORB-like ratios toward the value of the 1700°C oxide gabbro ultramylonite fraction (Figure 2). This is interpreted as the result of several likely effects including loss of magmatic helium and in situ radiogenic ^{4}He ingrowth.

[34] Table 4 shows the possible in situ accumulation of ^{4}He based on the measured U and Th

concentrations in our gabbro samples. Although some uncertainties remain as half of U and Th data are reported as upper limit, possible radiogenic ^{4}He ingrowth in 12Ma is enough to decrease their ^{3}He/^{4}He from that of MORB to the observed values. The helium composition of clinopyroxene in websterite 10K173R19 can be similarly explained. In the 700°C fraction it has ^{3}He/^{4}He 4.7 R_A and only 3×10^{-9} cm^3 STP/g of ^{4}He. This decrease of the ^{3}He/^{4}He ratio requires a ^{4}He accumulation of only 1.3×10^{-9} cm^3 STP/g over 12 Ma. Assuming that its Th and U concentrations are 10 ppb and 3 ppb with an acceptable mantle Th/U ratio (typically 3.5: e.g., *Ozima and Podosek* [1983]), possible in situ production of ^{4}He over 12 Ma reaches 7.8×10^{-9} cm^3 STP/g. Thus after at least partial escape of primordial helium, in situ ingrowth of radiogenic ^{4}He could explain the all observed ^{3}He/^{4}He ratio.

7.3. Atmospheric Contamination Processes

[35] The ^{36}Ar/^{22}Ne-^{132}Xe/^{22}Ne diagram may be a useful tool for discriminating among possible contaminants [*Kumagai and Kaneoka*, 2003] as three potential contaminants with atmospheric isotope ratios are clearly separated in the diagram: air, seawater, and seawater-equilibrated tholeiitic melt (Figure 5). The latter is a theoretical component calculated using noble gas solubilities in a tholeiitic magma [*Carroll and Webster*, 1994] equilibrated with seawater using Henry's law [*Ozima and Podosek*, 1983]. Although this component has an atmospheric isotopic composition it has elemental abundances quite different than either the atmosphere or seawater. In addition, simple two component mixing makes a linear trend in this diagram.

[36] All our gabbro and peridotite data follow a trend between the seawater-equilibrated tholeiitic magma component and another component represented by the lherzolite clinopyroxene separate. Therefore we conclude that the noble gas components of our samples were derived from mixing between these end-members. Three of the gabbros lie to the right of the mixing line offset toward the seawater component, and therefore also show some effects that can be ascribed to seafloor weathering. The low ^{40}Ar/^{36}Ar of the lherzolite clinopyroxene separate also supports some seawater contamination.

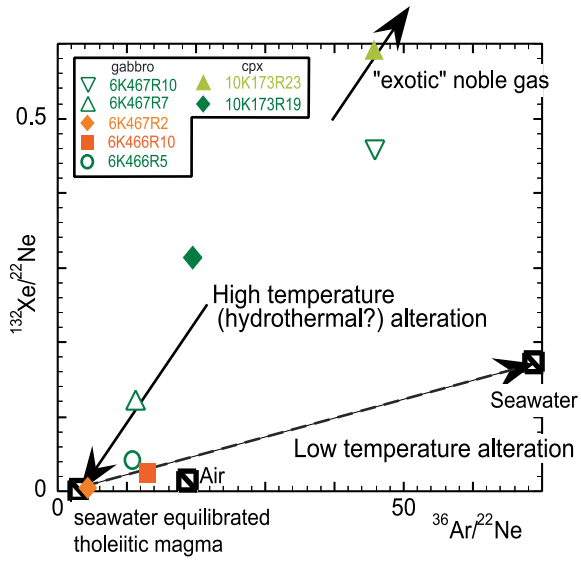

Figure 5. Relations between the ^{36}Ar/^{22}Ne and the ^{132}Xe/^{22}Ne for our samples. Values of air, seawater, and seawater-equilibrated tholeiitic magma are also shown. Here, the seawater-equilibrated tholeiitic magma is a theoretical component calculated using noble gas solubilities in a tholeiitic magma [*Carroll and Webster*, 1994, Figure 13] equilibrated with seawater using Henry's law [*Ozima and Podosek*, 1983, Table 7.6]. Symbols of samples are the same as Figure 1.

[37] The origin of the 'exotic' Xe enriched component has several possible explanations. This could be a mantle component, though the atmospheric isotope signatures of Ne and Xe do not support this. It could represent a severe fractionation of atmospheric noble gases occurring during alteration, but this component has also been seen in fresh hot spot lavas [e.g., *Patterson et al.*, 1990; *Harrison et al.*, 1999; *Althaus et al.*, 2003]. Accordingly the origin of this component remains undetermined.

[38] The direct equilibration of seawater and a MORB magma seems mechanically improbable. MORB melts can digest altered gabbro in the lower crust, however, this process seems to be most robust at fast spreading not slow-spreading ridges [*Michael and Schilling*, 1989]. A more likely explanation for this component in our gabbros is simply high-temperature hydrothermal alteration

by seawater circulating into the lower crust beneath the ridge axis. Our principle reservoir for helium and presumably the other noble gases appears to be green amphibole, which dominantly forms at middle amphibolite facies or higher in the Hole 735B gabbros [*Stakes*, 1991; *Stakes et al.*, 1991].

7.4. $^4He/^{40}Ar^*$

[39] $^4He/^{40}Ar^*$ ratios are frequently utilized as a tracer of magmatic components. Possible accumulation of in situ radiogenic ^4He and/or ^{40}Ar during 12 Ma, however, obscures the original $^4He/^{40}Ar^*$ ratios in most of the gabbros analyzed (Table 4). One exception is olivine gabbro 6K467R7, which contains the most abundant MORB-like helium in our suite. The $^4He/^{40}Ar^*$ ratio of this gabbro is 2.01, which is almost equivalent to the integrated production ratio of $^4He/^{40}Ar$ for 4.5 Ga of 2.1. In addition, this value is very close to the popping rock value of 1.6 [*Moreira et al.*, 1998]. Even taking into account possible in situ accumulation of ^{40}Ar for 12Ma, the $^4He/^{40}Ar^*$ value does not exceed 4. This is still lower than the present-day production ratio of $^4He/^{40}Ar$, 5.5.

[40] ^4He and ^{40}Ar ingrowth in the peridotites is negligible. Websterite 10K173R19 clinopyroxene shows almost identical $^4He/^{40}Ar^*$ with that of popping rock. This is consistent with an interpretation that it was produced by melt impregnation containing mantle noble gases. The high $^4He/^{40}Ar^*$ value of lherzolite (8.5) is difficult to explain at this point without more data.

8. Conclusions

[41] Oceanic gabbros and peridotites can preserve the primary magmatic helium signature of the MORB source, even within highly deformed and/or weathered rocks. Their maximum helium abundances exceed 1×10^{-7} cm^3 STP/g. Helium concentrations up to 10^{-6} cm^3 STP/g with MORB-like $^3He/^4He$ have also been estimated for oceanic lithosphere from ultramafic xenoliths [e.g., *Moreira and Kurz*, 2001]. Although those values are lower than those of MORB glasses by two to three orders of magnitude, these abundances are still significantly higher than those of crystalline

Table A1. Major and Selected Trace Elements[a]

Sample	SiO_2, %	Al_2O_3, %	Fe_2O_3, %	MnO, %	MgO, %	CaO, %	Na_2O, %	K_2O, %	TiO_2, %	P_2O_5, %	LOI, %	Total, %	Ba, ppm	Sr, ppm	Y, ppm	Sc, ppm	Zr, ppm	Be, ppm	V, ppm
6K467R10	52.73	17.11	6.54	0.125	8.45	11.83	3.45	0.12	0.308	0.01	0.05	100.72	4	180	8	38	12	–	155
6K467R7	50.78	17.26	4.48	0.096	9.09	13.86	2.69	0.08	0.442	0.02	0.36	99.15	3	153	9	38	22	–	157
6K467R2	47.43	14.02	15.12	0.216	4.44	8.88	4.07	0.21	4.743	0.05	0.57	99.74	10	181	18	48	51	–	623
6K466R10	54.51	15.70	10.51	0.130	2.80	7.59	5.85	0.12	1.330	0.75	0.53	99.82	14	242	117	35	1037	2	40
6K466R5	49.96	15.29	8.31	0.173	8.85	12.33	2.72	0.09	0.443	0.04	1.41	99.62	7	146	11	42	22	–	186
Detection limit													2	2	2	2	2	1	5

[a] Fusion ICP measurements with a flux of lithium metaborate/tetraborate were performed by Activation Laboratories Ltd., Ancaster, Canada: Report number 27067. Dashes indicate under detection limits.

Table A2. Trace Elements[a]

Sample[b]	V	Cr	Co	Ni	Cu	Zn	Ga	Ge	Rb	Sr	Y	Zr	Nb	Ag	Sn	Sb	Cs	Ba
6K467R10	161	47	39	73	112	67	16	1.4	-	181	9.1	16	1.1	-	-	−0.2	-	3
6K467R7	163	618	22	114	120	-	12	0.8	-	153	10.1	25	1.5	-	-	−0.2	-	-
6K467R2	632	−20	36	28	84	131	24	1.7	44	186	20.4	81	2.7	-	-	0.4	1.3	9
6K466R10	36	−20	25	32	104	84	28	1.8	5	244	121	1057	4.0	15.8	2	0.2	0.3	14
6K466R5	183	179	51	122	119	84	14	1.3	-	140	12.7	24	3.0	-	-	0.4	-	6
Detection limit	5	20	1	20	10	30	1	0.5	5	1	2	1	0.2	0.5	1	0.2	0.1	3

Sample[b]	La	Ce	Pr	Nd	Sm	Eu	Gd	Tb	Dy	Ho	Er	Tm	Yb	Lu	Hf	Ta	Tl	Pb	Th	U
6K467R10	0.40	1.28	0.23	1.69	0.82	0.613	1.25	0.26	1.67	0.36	1.01	0.137	0.90	0.131	0.6	-	-	5	-	-
6K467R7	0.78	2.42	0.40	2.50	1.05	0.623	1.47	0.29	1.83	0.39	1.09	0.151	0.98	0.144	1.0	-	-	-	-	-
6K467R2	0.98	3.31	0.59	4.08	1.95	1.43	2.81	0.57	3.65	0.78	2.23	0.317	2.10	0.324	2.6	0.10	0.55	-	-	0.24
6K466R10	16.6	54.6	8.87	54.4	18.2	6.90	21.7	3.83	23.0	4.76	13.0	1.81	11.9	1.75	20.3	0.06	0.11	5	0.17	0.23
6K466R5	1.20	4.57	0.52	3.29	1.34	0.756	1.90	0.36	2.31	0.50	1.36	0.195	1.25	0.186	1.0	-	0.21	6	0.28	0.13
Detection limit	0.05	0.05	0.01	0.05	0.01	0.005	0.01	0.01	0.01	0.01	0.01	0.005	0.01	0.002	0.1	0.01	0.05	5	0.05	0.01

[a] ICP-MS measurements were performed by Activation Laboratories Ltd., Ancaster, Canada: Report No 27067. Dashes indicate under detection limit.
[b] Given in ppm.

MORBs. Considering the large volumes of the lower crust and residual mantle, then, they are both important reservoirs of helium with the lower crust contributing equally or more than the upper crust to the helium budget. Both, however, are likely minor contributors (10% or less) compared to the residual mantle to the lithospheric helium budget. Given the assumption that the helium is highly incompatible, this is a surprising result. Recycling the oceanic lithosphere at subduction zones then should be considered in modeling mantle evolution.

[42] The noble gas abundances in our gabbros and peridotites are dominated by a component reflecting high temperature alteration and an exotic atmospheric component, though some of samples partly preserve a mantle derived noble gas signature indicated by $^{4}He/^{40}Ar^{*}$ ratios.

Appendix A. Chemical Analyses of Gabbros

[43] Chemical analyses of gabbros are shown in Tables A1 and A2.

Acknowledgments

[44] We would like to express our appreciation to Captain Ishida and the crews of the R/V *Kairei and Yokosuka*, operation teams of Shinkai 6500 and Kaiko ROV for their assistance throughout cruises. On-board and shore-based scientific teams are also appreciated owing to their contribution. We also thank to Philippe Sarda and Samuel Niedermann for their constructive reviews for early version of manuscript, and to Mark Kurz and Wolfgang Bach for their constructive discussions and useful comments. Yoshiro Nishio kindly provided his unpublished data. This study was supported by the following grants: the Grant-in-Aid for Scientific Research by the Ministry of Education, Culture, Sports, Science and Technology, Japan, (14540457), the Earthquake Research Institute cooperative research program (2001-G-06 and 2002-G-14) and the Grant C32 for Deep-Sea Research and Fellowship for Research Abroad from JAMSTEC to H.K., and NSF Grant OCE-9907630 to the Woods Hole Oceanographic Institution (WHOI). The expeditions were conducted as part of the Ocean Floor Geodynamics Program in JAMSTEC under MOU with WHOI.

References

Althaus, T., S. Niedermann, and J. Erzinger, Noble gases in olivine phenocrysts from drill core samples of the Hawaii Scientific Drilling Project (HSDP) pilot and main holes (Mauna Loa and Mauna Kea, Hawaii), *Geochem. Geophys. Geosyst.*, *4*(1), 8701, doi:10.1029/2001GC000275, 2003.

Brooker, R. A., Z. Du, J. D. Blundy, S. P. Kelley, N. L. Allan, B. J. Wood, E. M. Chamorro, J.-A. Wartho, and J. A. Purton, The 'zero charge' partitioning behaviour of noble gases during mantle melting, *Nature*, *423*, 738–741, 2003.

Burnard, P., D. Graham, and G. Turner, Vesicle-specific noble gas analyses of "popping rock": Implications for primordial noble gases in Earth, *Science*, *276*, 568–571, 1997.

Carroll, M. R., and J. D. Webster, Solubilities of sulfur, noble gases, nitrogen, chlorine and fluorine in magmas, in *Volatiles in Magmas*, edited by M. R. Carroll and J. R. Holloway, pp. 231–279, Mineral. Soc. Am., Washington, D. C., 1994.

Dick, H. J. B., Abyssal peridotites, very slow spreading ridges and ocean ridge magmatism, in *Magmatism in the Ocean Basins*, edited by A. D. Saunders and M. J. Norry, *Geol. Soc. Spec. Publ.*, *42*, 71–105, 1989.

Dick, H. J. B., J. H. Natland, H. Kinoshita, P. Robinson, C. MacLeod, A. Kvassnes, and MODE'98, and ODP Leg Scientific Parties, The nature of intrusion and melt transport in the lower ocean crust at an ultraslow spreading ridge, paper presented at the Ninth Annual V.M. Goldschmidt Conference, Geochem. Soc., Cambridge, Mass., 1999a.

Dick, H. J. B., et al., Proceedings of the Ocean Drilling Program, Initial Reports [CD-ROM], 176, Ocean Drill. Program, College Station, Tex., 1999b.

Dick, H. J. B., et al., A long in situ section of the lower ocean crust: Results of ODP Leg 176 drilling at the southwest Indian Ridge, *Earth Planet. Sci. Lett.*, *179*, 31–51, 2000.

Drescher, J., T. Kirsten, and K. Schäfer, The rare gas inventory of the continental crust recovered by the KTB continental deep drilling project, *Earth Planet. Sci. Lett.*, *154*, 247–263, 1998.

Dunai, T. J., and D. Porcelli, Storage and transport of noble gases in the subcontinental lithosphere, in *Noble Gases in Geochemistry and Cosmochemistry*, edited by D. Porcelli et al., pp. 371–409, Mineral Soc. Am., Washington, D. C., 2002.

Dymond, J., and L. Hogan, Noble gas abundance patterns in deep-sea basalts: Primordial gases from the mantle, *Earth Planet. Sci. Lett.*, *20*, 131–139, 1973.

Graham, D. W., Noble gas isotope geochemistry of Mid-Ocean Ridge and Ocean Island Basalts: Characterization of mantle source reservoirs, in *Noble Gases in Geochemistry and Cosmochemistry*, edited by D. Porcelli et al., pp. 247–318, Mineral. Soc. Am., Washington D. C., 2002.

Hanyu, T., I. Kaneoka, and K. Nagao, Noble gas study of HIMU and EM ocean island basalts in the Polynesian region, *Geochim. Cosmochim. Acta*, *63*, 1181–1201, 1999.

Harrison, D., P. Burnard, and G. Turner, Noble gas behaviour and composition in the mantle: Constraints from the Iceland Plume, *Earth Planet. Sci. Lett.*, *171*, 199–207, 1999.

Honda, M., and D. B. Patterson, Systematic elemental fractionation of mantle-derived helium, neon, and argon in mid-oceanic ridge glasses, *Geochim. Cosmochim. Acta*, *63*, 2863–2874, 1999.

Hosford, A., M. Tivey, T. Matsumoto, H. Dick, H. Schouten, and H. Kinoshita, Crustal magnetization and accretion at the

Southwest Indian Ridge near the Atlantis II fracture zone, 0–25 Ma, *J. Geophys. Res.*, *108*, 2169–2191, 2003.

John, B. E., D. A. Foster, J. M. Murphy, C. M. Fanning, and P. Copeland, Quantitative age and thermal history of in situ lower oceanic crust -Atlantis Bank, SW Indian Ridge, paper presented at the SWIR workshop, Inter Ridge, Southampton, United Kingdom, 17–19 April 2002.

Johnson, K. T. M., and H. J. B. Dick, Open system melting and the temporal and spatial variation of peridotite and basalt compositions at the Atlantis II Fracture Zone, *J. Geophys. Res.*, *97*, 9219–9241, 1992.

Klein, E. M., and C. H. Langmuir, Global correlations of ocean ridge basalt chemistry with axial depth and crustal thickness, *J. Geophys. Res.*, *92*, 8089–8115, 1987.

Kumagai, H., and I. Kaneoka, Variations of noble gas abundances and isotope ratios in a single MORB pillow, *Geophys. Res. Lett.*, *25*, 3891–3894, 1998.

Kumagai, H., and I. Kaneoka, Relationship between submarine MORB glass textures and atmospheric component of MORBs, *Chem. Geol.*, *200*, 1–24, 2003.

Matsumoto, T., H. J. Dick, and ABCDE Cruise scientific party, In-situ observation of the lower crust and upper mantle lithology in Atlantis Bank, SWIR: Results from ABCDE Cruise, *Eos Trans. AGU*, *83*(47), Fall Meet. Suppl., Abstract T11A-1239, 2002.

Michael, P. J., and J.-G. Schilling, Chlorine in mid-ocean ridge magmas: Evidence for assimilation of seawater-influenced components, *Geochim. Cosmochim. Acta*, *53*, 3131–3143, 1989.

Moreira, M., and M. D. Kurz, Subducted oceanic lithosphere and the origin of the 'high μ' basalt helium isotopic signature, *Earth Planet. Sci. Lett.*, *189*, 49–57, 2001.

Moreira, M., J. Kunz, and C. Allègre, Rare gas systematics in popping rock: Isotopic and elemental compositions in the upper mantle, *Science*, *279*, 1178–1181, 1998.

Natland, J. H., and H. J. B. Dick, Formation of the lower ocean crust and the crystallization of gabbroic cumulates at a very slowly spreading ridge, *J. Volcanol. Geotherm. Res.*, *110*, 191–233, 2001.

Ozima, M., and F. A. Podosek, *Noble Gas Geochemistry*, 367 pp., Cambridge Univ. Press, New York, 1983.

Patterson, D. B., M. Honda, and I. McDougall, Atmospheric contamination: A possible source for heavy noble gases in basalts from Loihi seamount, Hawaii, *Geophys. Res. Lett.*, *17*, 705–708, 1990.

Porcelli, D., and C. J. Ballentine, Models for the distribution of terrestrial noble gases and evolution of the atmosphere, in *Noble Gases in Geochemistry and Cosmochemistry*, edited by D. Porcelli et al., pp. 411–480, Mineral Soc. Am., Washington, D. C., 2002.

Porcelli, D., C. J. Ballentine, and R. Wieler (Eds.), *Noble Gases - in Geochemistry and Cosmochemistry*, 844 pp., Mineral Soc. Am., Washington, D. C., 2002.

Sarda, P., and M. Moreira, Vesiculation and vesicle loss in mid-ocean ridge basalt glasses: He, Ne, Ar elemental fractionation and pressure influence, *Geochim. Cosmochim. Acta*, *66*, 1449–1458, 2002.

Sarda, P., M. Moreira, T. Staudacher, J.-G. Schilling, and C. J. Allègre, Rare gas systematics on the southernmost Mid-Atlantic Ridge: Constraints on the lower mantle and Dupal source, *J. Geophys. Res.*, *105*, 5973–5996, 2000.

Stakes, D. S., Oxygen and hydrogen isotope compositions of oceanic plutonic rocks: High-temperature deformation and metamorphism of oceanic layer 3, in *Stable Isotope Geochemistry: A Tribute to Samuel Epstein*, edited by H. P. Taylor Jr., J. R. O'Neil, and I. R. Kaplan, pp. 77–90, Geochem. Soc., Cambridge, Mass., 1991.

Stakes, D., C. Mével, M. Cannat, and T. Chaput, Metamorphic stratigraphy of Hole 735B, *Proc. Ocean Drill. Program Sci. Results*, *118*, 153–180, 1991.